Short title: Bundle sheath extensions and leaf plasticity

Corresponding author details:

Agustin Zsögön

Universidade Federal de Viçosa, Brazil

Phone: +55 31 3899 2592

Fax: +55 31 3899 4139

agustin.zsogon@ufv.br

Title: Bundle sheath extensions in tomato affect leaf phenotypic plasticity in response to irradiance

Authors: Maria Antonia M. Barbosa[1], Daniel H. Chitwood[2]; Aristéa A. Azevedo[1]; Wagner L. Araújo[1,4]; Samuel C. V. Martins[1]; Dimas M. Ribeiro[1]; Lázaro E. P. Peres[3]; Agustin Zsögön[1*]

Affiliations

[1]*Departamento de Biologia Vegetal, Universidade Federal de Viçosa, CEP 36570-900, Viçosa, MG, Brazil*

[2]*Independent Researcher, Santa Rosa, CA 95409 USA*

[3]*Laboratory of Hormonal Control of Plant Development. Departamento de Ciências Biológicas, Escola Superior de Agricultura "Luiz de Queiroz", Universidade de São Paulo, CP 09, 13418-900, Piracicaba, SP, Brazil*

[4]*Max-Planck Partner group at the Departamento de Biologia Vegetal, Universidade Federal de Viçosa, 36570-900, Viçosa, MG, Brazil.*

Email addresses:

MAMB, mabarbosa483@gmail.com

DHC, dhchitwood@gmail.com

AAA, aristea.azevedo@gmail.com

WLA, wlaraujo@ufv.br

SCVM, samuel.martins@ufv.br

DMR, dimas.ribeiro@ufv.br

LEPP, lazaro.peres@usp.br

Summary: The presence of bundle sheath extensions in tomato influences various leaf physiological and structural parameters in response to irradiance

Author contributions

M.A.M.B. and D.H.C. conducted experiments and prepared Figures and/or tables. A.A.A., W.L.A. D.M.R., S.C.V.M. and L.E.P.P. designed experiments, contributed reagents/materials/analysis tools and reviewed drafts of the paper. A.Z. conceived and designed the experiments, analyzed the data and wrote the paper with contributions from the other authors.

Corresponding author: AZ, agustin.zsogon@ufv.br

Abstract

Coordination between structural and physiological traits is key to plants' responses to environmental fluctuations. This is especially relevant to leaf hydraulics, as plant face constant imbalances between water supply and demand. In heterobaric leaves, bundle sheath extensions (BSEs) increase water transport capacity, as measured by leaf hydraulic conductance (K_{leaf}). The *obscuravenosa* (*obv*) mutation, found in many commercial tomato varieties, leads to absence of BSEs. We examined structural and physiological traits of tomato heterobaric and homobaric (*obv*) near-isogenic lines (NILs) grown at two different irradiance levels. We found that K_{leaf}, minor vein density and stomatal pore area index decrease with shading in heterobaric but not in homobaric leaves, which show similarly lower values in both conditions. Whole plant dry mass, as well as fruit yield, were altered by irradiance but not by genotype. We propose that BSEs confer plasticity in traits related to leaf structure and function in response to irradiance levels and might act as a hub integrating water supply and demand. Similar plant growth and yield in both NILs suggests that other developmental pathways can compensate for the lack of BSEs. This is in line with the fact that *obv* is not a deleterious mutation, and probably confers some adaptive advantage, as it was selected during commercial tomato breeding.

Introduction

The plethora of structural variation found in leaves has been interpreted either as closely tracking environmental conditions or a relatively loose connection between form and function, which has allowed for high plasticity provided a minimal level of performance is maintained (Niklas, 1992). The coordination of leaf structure with hydraulic design is of paramount importance for plant function, acclimation to the environment, and ecological distribution (Nicotra et al., 2008; Nicotra et al., 2011). The rate of water transport through the leaf is a fine balancing act dictated by resource supply-and-demand dynamics and constrained by the laws of biophysics (Brodribb, 2009; Buckley et al., 2016).

Water flow through the plant body is analogous to an electric circuit, with a series of additive resistances (R) between the soil and the atmosphere. In this system, the leaf constitutes a hydraulic bottleneck and a strong determinant of whole-plant performance (Sack and Holbrook, 2006). R_{leaf} is dynamic and can vary with time of day, irradiance, temperature, and water availability (Prado and Maurel, 2013). The efficiency of water transport through the leaf is measured as K_{leaf}, the inverse function of R_{leaf}. Other leaf architectural traits (*e.g.* leaf thickness, stomatal pore area, lamina margin dissection, among others) have been dissected and are also well-known to reciprocally influence K_{leaf} (Sack and Frole, 2006).

In particular, vein structure and patterning play a critical role in water distribution within plants (Sack et al., 2012). Water flow through the leaf occurs via xylem conduits within the vascular bundles, which upon entering the lamina from the petiole rearrange into major and minor veins. The midrib (primary), secondary, and tertiary veins are involved mainly in water supply, whereas higher order veins (quaternary and above) are involved in water distribution throughout the lamina (Sack and Scoffoni, 2013). Higher K_{leaf} values are associated with a greater midrib diameter, and higher minor vein density (Brodribb et al., 2007). Water movement outside the xylem is more difficult to study and quantify, but the extra-xylematic pathway may contribute as much to R_{leaf} as the xylem pathways in some species (Scoffoni, 2015). However, it is still unclear whether this flow occurs through symplastic or apoplastic pathways, or a combination of both (Buckley et al., 2015).

Upon leaving the xylem, water has to transit through the bundle sheath, a layer of compactly arranged parenchymatic cells surrounding the vasculature (Esau, 1977). Bundle sheaths could behave as flux sensors or 'control centers' of leaf water transport, and they are most likely responsible for the high dependence of K_{leaf} on temperature and irradiance (Leegood, 2008; Ohtsuka et al., 2017). Vertical layers of colorless cells connecting the vascular bundle to the epidermis are present in many eudicotyledons. These so-called bundle sheath extensions (BSEs) are most commonly found in minor veins, but can occur in veins of any order depending on the species (Wylie, 1952). A topological consequence of the presence of BSEs is the formation of compartments in the lamina, which restricts lateral gas flow and thus allows compartments to maintain gas exchange rates independent of one another (Buckley et al., 2011). Such leaves, and by extension the species possessing them, are therefore called 'heterobaric', as opposed to 'homobaric' species lacking BSEs.

Large taxonomic surveys have demonstrated that heterobaric species tend to occur more frequently in sunny and dry sites or in the upper stories of climax forests (Kenzo et al., 2007), so it was hypothesized that BSEs could fulfill an ecological role by affecting mechanical and physiological parameters in the leaf (Terashima, 1992). Some of these functions, such as providing mechanical support (Read and Stokes, 2006), protecting the leaf from mechanical damage or restricting the spread of disease (Lawson and Morison, 2006), remain hypothetical. Other functions, however, have been proven through meticulous experimental work, suggesting that the existence of BSEs could be adaptive (Buckley et al., 2011). For instance, lateral propagation of ice in the lamina was precluded by the sclerenchymatic BSEs in *Cinnamomum canphora* L (Hacker and Neuner, 2007). Moreover, hydraulic integration of the lamina is increased by BSEs, which connect the vascular bundle to the epidermis and, therefore, reduce the resistance in the water path between the supply structures (veins) and the water vapor outlets (stomata) (Zwieniecki et al., 2007). Finally, photosynthetic assimilation rates are increased in leaves with BSEs, due to their optimization of light transmission within the leaf blade (Karabourniotis et al., 2000; Nikolopoulos et al., 2002).

Most of the above studies addressing the function of BSEs are generally based on large-scale multi-species comparisons, which restricts the conclusions to a statistical effect. Many structural and hydraulic leaf traits are strongly co-ordinated and co-selected, therefore reducing

the discriminating power of analyses involving species of different life forms and ecological background. We have previously characterized a mutant that lacks BSEs in the otherwise heterobaric species tomato (*Solanum lycopersicum* L.) (Zsögön et al., 2015). The homobaric mutant *obscuravenosa* (*obv*) reduces K_{leaf} and stomatal conductance but does not impact global carbon economy of the plant. Here, we extend our observations to plants grown under two contrasting irradiance levels, which are known to influence both leaf structure (Oguchi et al., 2003; Oguchi et al., 2005; Oguchi et al., 2006) and K_{leaf} (Scoffoni et al., 2008; Guyot et al., 2012). We investigated whether the presence of BSEs could have an impact on the highly plastic nature of leaf development and function in response to different irradiance levels. By assessing a series of leaf structural and physiological parameters in tomato cv Micro-Tom (MT) and the near-isogenic *obv* mutant, we provide evidence of the potential role of BSEs in the coordination of leaf structure and hydraulics in response to growth irradiance. Finally, we analysed whether dry mass accumulation and tomato fruit yield are affected by the presence of BSEs and irradiance in two different tomato genetic backgrounds (cv MT and M82). We discuss the potential role of BSEs in the coordination of hydraulics with leaf structure in response to the light environment.

Results

This study was performed on two tomato genetic backgrounds, cultivars Micro-Tom (MT) and M82, and their *obscuravenosa* (*obv*) mutant near-isogenic lines (NILs). First, we performed a microscopic analysis of terminal leaflet cross-sections to confirm that MT harbors bundle sheath extensions (BSEs) in the translucent major veins of fully-expanded leaves (Fig. S1). The *obv* mutant, on the other hand, lacks these structures. We further conducted a water+dye infiltration assay in the lamina, proving that, under similar pressure, intercellular spaces of the *obv* mutant are flooded almost twice (86.1% vs 47.3%, p=0.012) as much as for MT (Fig. S2). Dry patches are observed in MT, which shows that the presence of BSEs in secondary veins creates physically isolated compartments in the lamina (Fig. S2). We therefore follow the established nomenclature of ‘heterobaric’ for MT and ‘homobaric’ for *obv*.

Irradiance level alters leaf shape and structural parameters differentially in heterobaric and homobaric leaves

We began by conducting an analysis of leaflet shape between the treatments. We used an Elliptical Fourier Descriptor (EFD) analysis (Iwata and Ukai, 2002) to determine how light treatment and the *obv* mutation affect leaf shape, independent from size. This method treats a closed contour as a wavelength that is decomposed into a Fourier harmonic series to quantify shapes (Iwata et al., 1998; Iwata and Ukai, 2002). A Principal Component Analysis (PCA) on harmonic coefficients contributing to symmetric shape variation separates MT and *obv* genotypes, but fails to show large differences in shape attributable to light treatment (Fig. 1). To visualize the effects of genotype and light, we superimposed mean leaflet shapes from each genotype-light combination (Fig. 1). *obv* imparts a wider leaflet shape relative to MT, regardless of light treatment. Light treatment does not discernibly affect leaflet shape. These results are similar to previous studies in tomato and wild relatives in which the effects of the shade avoidance response on leaf shape were negligible compared to genotypic effects (Chitwood et al., 2012; Chitwood et al., 2015).

Sun leaves had reduced total specific leaf area (SLA) compared to shade leaves in both MT and the *obv* mutant (Fig. 1). Shading increased SLA values by 101% and 62% for MT and *obv* plants, respectively, when compared to plants in the sun treatment (P=0.0001). Terminal leaflets of fully expanded MT sun leaves had 62% higher perimeter/area than MT shade leaves, unlike *obv* where no difference was found between irradiance levels (Fig. 1). Perimeter^2/area, which, unlike perimeter/area is a dimensionless measure of leaf shape (and, therefore, does not inherently scale with size), was strongly dependent on genotype and not influenced by irradiance (Fig. 1). Leaf lamina thickness was greater in sun than in shade leaves, with no differences between genotypes (Fig. 1).

Growth irradiance alters leaf hydraulic conductance (K_{leaf}) in heterobaric but not in homobaric leaves

K_{leaf} is a key parameter determining plant water relations, as it usually scales up to the whole plant level. It is a measure of how much water loss through transpiration a leaf can sustain

at a given water potential. We previously showed that K_{leaf} is reduced in the homobaric mutant *obv* compared to MT (Zsögön et al., 2015). Here, we assessed K_{leaf} in heterobaric and homobaric leaves grown in sun/shade conditions (Fig. 2). Shading decreased K_{leaf} in the heterobaric genotype: MT shade leaves had 41% lower K_{leaf} than sun leaves (14.95 ± 1.91 *vs* 25.36 ± 1.32 mmol H_2O m^{-2} s^{-1} MPa^{-1}). Homobaric and heterobaric leaves in the M82 tomato background showed consistently similar results (Fig. S3), where shade leaves had 36% lower K_{leaf} than sun leaves (18.72 ± 0.59 *vs* 29.6 ± 2.1 mmol H_2O m^{-2} s^{-1} MPa^{-1}) (Fig. S4). The *obv* mutant, on the other hand, showed similarly low K_{leaf} values in either condition and in both genetic backgrounds (MT sun: 17.86 ± 1.26 *vs* shade: 17.87 ± 2.14 mmol H_2O m^{-2} s^{-1} MPa^{-1}; M82: sun: 19.19 ± 2.24 *vs* shade: 19.17 ± 2.67 mmol H_2O m^{-2} $s^{-1}MPa^{-1}$) (Fig. 2, S4). The results were consistent between tomato backgrounds, even though both cultivars differ in leaf lamina size and other leaf structural parameters.

Shading reduces stomatal conductance in heterobaric leaves, whereas homobaric leaves maintain similarly low values under both conditions

We analysed the response of photosynthetic assimilation rate (A) to varying internal partical pressure of CO_2 in the substomatal cavity (C_i) on fully expanded terminal leaflets attached to plants growing in the greenhouse under sun or shade treatments (Table 2). The apparent maximum carboxylation rate of Rubisco (V_{cmax}), the maximum potential rate of electron transport used in the regeneration of RuBP (J_{max}) and the speed of use of triose-phosphates (TPU) were reduced by 20.0 (P=0.0696), 20.2 (P=0.01) and 21.1% (P=0.006), respectively, for shade compared to sun MT plants. In *obv*, the respective drop between sun and shade plants the same parameters was 10.0, 7.0 and 6.0% respectively (Table 3).

The hyperbolic relationship between A and g_s measured at ambient CO_2 was not altered by irradiance level (Figure 3). The lower limit for g_s values was remarkably similar between genotypes in both light conditions (~0.2 mol m^{-2} s^{-1}). Shading, however, drove a 30% decrease in g_s in MT (P=0.029) with a concomitant limitation to A (P=0.023) (Table 3), mostly by reducing the variability for this parameter in MT (Fig. 3). In the *obv* mutant, g_s was lower in the sun (similar value to shade MT) and remained essentially unchanged by shading (P=0.9293), as did A (P=0.6350). The A/g_s ratio, or intrinsic transpiration efficiency (WUE_i), was therefore higher

in homobaric *obv* plants than in heterobaric MT under both irradiance levels. A similar, although not statistically significant difference (possibly owing to the lower number or replicates, n=5) was found in M82 (Fig. S4).

Dark respiration was not affected by genotype or irradiance level (Table 2). The chlorophyll fluorescence analyses did not reveal any differences between genotypes in the photosynthetic efficiency of light utilization (Table S1).

Stomatal Pore Area Index is altered by irradiance in heterobaric but not homobaric leaves

Stomatal conductance (g_s) is influenced by the maximum stomatal conductance (g_{max}), which is in turn determined by stomatal size and number. To further explore the basis for the differential g_s response to irradiance between genotypes, we analysed stomatal traits in terminal leaflets of fully expanded leaves. Stomatal pore area index (SPI, a dimensionless measure of the combined stomatal density and size) was increased only in MT sun leaves (Fig. 4), compared to all the other treatments. Guard cell length, which is linearly related to the assumed maximum stomatal pore radius, was greater in *obv* than in MT and was not affected by the irradiance levels (Fig. 4). Thus, the main driver of the difference in SPI was stomatal density, particularly on the abaxial side, which represents a quantitatively large contribution (Fig. 4). Adaxial stomatal density was reduced in the shade in both genotypes, with no differences between them within irradiance levels (Fig. 4).

Intercellular air spaces and vein density are differentially altered by irradiance levels in heterobaric and homobaric leaves

Light microscopy analyses of leaf cross-sections revealed differences in leaf anatomy dependent on genotype and irradiance level. Lamina thickness was reduced by shading in both genotypes, with no difference between them (Fig. 5). This results is in good agreement with the reduced specific leaf area (SLA) in shade-grown plants (Fig. 1). Thickness of the abaxial epidermis, a proxy for stomatal depth, did not vary in MT between irradiance levels, but was reduced in shaded *obv* plants (Fig. 5). Intercellular air spaces in the lamina comprised close to 10% of the cross-sectional area in MT and *obv* plants grown in the sun, but when plants were

grown in the shade, it was increased to 12% (P=0.0658) in MT and 17% (P=0.0036) in *obv*. As venation is a key trait that influences water distribution in the lamina, we assessed minor vein density (tertiary and higher orders) and observed a genotype×irradiance interaction (Figure 5). Vein density was reduced in both genotypes by shading, but more strongly in MT than in *obv* (Fig. 5).

Carbohydrate and pigment contents in heterobaric and homobaric leaves under different irradiance

To ascertain whether the anatomical and physiological differences described above impacted leaf biochemistry, we assessed a basic set of compounds related to primary cell metabolism in MT and *obv* under both sun and shade conditions, along with photosynthetic pigments (Table S2). As expected, carbohydrate concentrations were strongly matched with irradiance level (Table S2). Shading promoted a decrease (P=0.001) in starch content in both genotypes, but of a considerable greater magnitude in MT (-45.0%) than in *obv* (-28.5%) compared to sun plants (Table S2). Glucose and fructose were increased in the shade, with no difference between genotypes. The chlorophyll a/b ratio was similar for all plants (P=0.24). A slight increase in carotenoid (CAR) levels was found in *obv* shade plants (P=0.004) (Table S2).

Morphological differences between heterobaric and homobaric plant grown under different irradiances do not affect dry mass accumulation or fruit yield

To determine whether the anatomical and physiological differences described above scale up to the whole-plant level and affect carbon economy and agronomic parameters of tomato, we determined dry mass and fruit yield in sun- and shade-grown plants of MT and *obv*. There was no difference in plant height (P=0.82) or in the number of leaves before the first inflorescence (P=0.82), for plants of either genotype in both light intensities (Table 3). There was a decrease of 29.1% and 26.0% in stem diameter in MT and *obv* plants respectively, for the shade treatment compared to sun (P=0.001). This proves that the shade treatment imposed was enough to cause a weak etiolation, although not affecting plant height, probably due to the determinate growth habit of the MT background (Campos et al., 2010). Leaf insertion angle relative to the stem,

however, was steeper in the *obv* mutant under both irradiance conditions. Different light intensities did not change leaf dry weight (P=0.25), however, *obv* plants showed a 24.3% reduction in stem dry weight (P=0.006), 46.4% in root dry weight (P=0.0002) and 31% in total dry weight (P=0.01) when compared to the sun treatment. The results were similar for MT, so no changes in dry mass allocation pattern were discernible between genotypes. Side branching is one of the most common gross morphological parameters affected by shading. A decrease (P=0.0001) in side branching was found in both genotypes upon shade treatment, with no differences between them (Fig. S5).

The results described in this section revealed that vegetative dry mass accumulation was affected solely by irradiance level with no influence of the genotype (nor therefore of the BSE). To ensure that potential differences arising from altered partitioning or allocation of carbon were not overlooked, we also assessed reproductive traits, *i.e.* parameters related to tomato fruit yield. Average tomato fruit yield per plant was reduced by shading, but did not differ between genotypes, in two different genetic backgrounds (MT and M82) within each irradiance condition (Table S3). The content of soluble solids in the fruit (Brix), a parameter of agronomic interest, was consistently stable across genotypes and treatments.

Discussion

Here, we compared different genotypes of a single herbaceous species (tomato) varying for a defined and ecologically relevant structural feature of the leaves: the presence of BSEs. The *obv* mutant lacks BSEs and thus produces homobaric leaves, compared to tomato cultivar Micro-Tom (MT), which has heterobaric leaves (Zsögön et al., 2015). We investigated the effect of irradiance on a series of developmental and physiological parameters. We hypothesized that homobaric leaves, lacking a key physical feature that increases leaf hydraulic integration, would exhibit less plasticity in their response to environmental conditions than heterobaric leaves.

K_{leaf} was higher in heterobaric than in homobaric sun plants, consistent with the notion that BSEs act as an additional extra-xylematic pathway for the flow of liquid water (Buckley et al., 2011; Zsögön et al., 2015). On the other hand, homobaric and heterobaric shade leaves showed similar K_{leaf} values indicating that the presence of BSEs differentially affects leaf

hydraulic architecture in response to irradiance. K_{leaf} is dynamically influenced by irradiance over different time scales, in the short-term by yet unknown factors (Scoffoni et al., 2008), and in the long-term by developmental plasticity altering leaf structural and physiological traits (Scoffoni et al., 2015). Recently, Buckley et al. (2015) modelled the influence of BSEs on K_{leaf} and found that their presence could increase K_{leaf} by about 30%. Interestingly, under high irradiance (sun), K_{leaf} was *c.* 30% higher in MT in comparison to *obv* plants which is in line with the Buckley et al. (2015) modelling; however, no difference in K_{leaf} was found in both genotypes under shade. A possible role for aquaporins present in the BS and/or the mesophyll has been proposed (Cochard et al., 2007) and it is known that aquaporins have their expression reduced under shade (Laur and Hacke, 2013). Thus, it is seems reasonable to assume that other K_{leaf} components were downregulated under shade, masking the contribution of BSEs to K_{leaf}.

A large set of physiological and structural traits are known to shift in tandem in response to irradiance (Scoffoni et al., 2015). Particularly, plants developing under high light conditions present a higher thermal energy load, which is dissipated mainly through leaf transpiration (Martins et al., 2014). In order to achieve higher transpiration rates, there must be a balance between hydraulic supply and demand, where vein patterning is coordinated with stomatal distribution to optimize resource utilization (Brodribb and Jordan, 2011). Such coordination is known to occur across vascular plant species, but exactly how veins and stomata "communicate" with each other remains to be elucidated (Carins Murphy et al., 2017). In this sense, one of the proposed roles of BSEs is to act as a hydraulic linkage route between the vascular bundles and the epidermis, integrating these otherwise separated tissues (Zwieniecki et al., 2007). Indeed, we found that the presence of BSEs allowed a proper coordination between veins and stomata, upregulating hydraulic supply and demand under high light (Fig. 6). On the other hand, in genotypes lacking BSEs, the abaxial stomata and vein densities remained unchanged (Fig. 6). This observation points to an additive hydraulic signal, modulated by BSEs, influencing stomata development. Another potential structural benefit of BSEs would be the provision of mechanical support (like a suspension bridge), in turn partially relieving the vein system from such duty and allowing heterobaric leaves greater flexibility in vein spacing compared to homobaric ones. Thus, we propose that the presence of BSEs can be usefully conceptualized as a hub coordinating trait plasticity in response to irradiance (Fig. 7).

Plants lacking BSEs responded to irradiance by altering the amount of intercellular air spaces in the leaf. The increased amount of intercellular air spaces is a typical response to shade acclimation where a potential benefit would be an enhanced leaf absorptance due to greater internal light scattering in spongy mesophyll (Lambers et al., 2008). Interestingly, heterobaric leaves would benefit less from such increase in leaf absorptance because BSEs are thought to optimize light transmission within the leaf blade (Karabourniotis et al., 2000; Nikolopoulos et al., 2002); this would partially explain why MT plants did not increase their intercellular air spaces as much as *obv* plants. In addition, the amount of intercellular air spaces is linearly related to the total surface area of chloroplasts facing the intercellular spaces per unit leaf area, and is thus a determinant of the diffusional resistance within the leaf blade (Evans and vonCaemmerer, 1996). Given that homobaric leaves derive a physiological advantage from the gaseous integration of the leaf lamina (Pieruschka et al., 2006), it is noteworthy that their response to irradiance involves increased plasticity for a structural trait that increases intracellular CO_2 conductance (Flexas et al., 2013).

A limitation in the study of the coordination of leaf structural and physiological traits is that most of the work on the topic has been conducted addressing interspecific level relations, with less work published at the intraspecific level. Many simple and relevant trait-trait correlations are potentially obscured by the analysis of multi-species mean values (Lloyd et al., 2013). Breaking down individual traits within single species of a given life form and then adding up their contributions is an alternative. Available mutants in model organisms are a suitable material for such an approach (Carvalho et al., 2011). When the genetic basis for the *obv* mutant is found, it will be possible to generate (a) novel allelic variation and, therefore, a wider range of phenotypes than the two currently available, and (b) inducible gene constructs that can be used to alter the ontogenetic trajectory of BSEs. Such a genetic toolkit to manipulate leaf developmental plasticity would greatly widen the scope of feasible experimental work, which has hitherto been restricted to relatively wide inter-specific comparisons (Liakoura et al., 2009; Inoue et al., 2015).

An open question is why the structural and physiological effects of the absence of BSEs in a leaf do not scale up to whole-plant carbon economy and growth. In other words, under what set of environmental conditions (if there is one) does the presence or absence of BSEs result in a significant fitness (*i.e.* survival and reproduction) difference between genotypes? The *obv*

mutation has been incorporated by breeders in many tomato cultivar and hybrids (Jones et al., 2007), suggesting that it can confer some agronomic advantage. Here, using NILs, we show that *obv* does not entail yield penalty but we fail to show any advantage of the trait, at least in the conditions tested. The present work was limited to analyzing the effect of quantitative differences in irradiance and thus represents only a starting point to answering this question. The strong plasticity of plant development in response to irradiance (all other conditions being similar) could be the reason why potential economic differences between genotypes were canceled out within a given light environment. It is not possible to rule out that stronger quantitative differences in irradiance level than the one tested here could tilt the phenotypic and fitness scales in favor of one of the leaf designs (*i.e.* heterobaric/homobaric). Alternatively, other variables (*e.g.* water and nitrogen availability, ambient CO_2 concentration) and combinations thereof could result in conditions where the difference in leaf structure scales up to the whole plant level. Given the presumed hydraulic benefit of BSEs, situations where the hydraulic system is probed at most (*e.g*. high vapour pressure deficit conditions) might be useful to maximize the benefit of 'being' heterobaric. We endeavor to address these questions in the near future.

Conclusions

The presence of BSEs in heterobaric tomato plants is coordinated with variation in both structural and physiological leaf traits under different growth irradiance levels (sun/shade). A homobaric mutant where BSEs are absent shows a pattern of responses whereby the plastic response is shifted to a different set of traits than the one affected in heterobaric plants. This variation, nevertheless, allows homobaric plants to maintain leaf physiological performance and growth under both irradiance conditions and results in the carbon economy and allocation of either genotype being indistinguishable within each irradiance level. Further insight into this fascinating complexity will come when the genetic basis for BSE development is unveiled.

Materials and Methods

Plant material

Seeds of the tomato (*Solanum lycopersicum* L.) cv Micro-Tom (MT) and cv M82 were donated by Dr Avram Levy (Weizmann Institute of Science, Israel) and the Tomato Genetics

Resource Center (TGRC, Davis, University of California, CA, USA), respectively. The introgression of the *obscuravenosa* (*obv*) into the MT genetic background was described previously (Carvalho et al., 2011). The model tomato M82 cultivar harbors the *obv* mutation, so the experiments were performed on F1 lines obtained by crosses between MT and M82. Both F1 lines have 50% MT and 50% M82 genome complement, differing only in the presence or absence of BSEs (Fig. S3; described in Table 1).

Growth conditions

Data were obtained from two independent assays, similar results were found both times. Plants were grown in a greenhouse in Viçosa (642 m asl, 20° 45' S; 42° 51' W), Minas Gerais, Brazil, under semi-controlled conditions. Micro-Tom (MT) background plants were grown during the months of May to August of 2016 in temperature of 24/20°C, 13/11h (day/night) photoperiod. Plants in the M82 background were cultivated during the months of September to December of 2016 with temperature of 26/22°C, 12/12h (day/night) photoperiod. Seeds were germinated in polyethylene trays with commercial substrate Tropostrato® and supplemented with 1g L^{-1} 10:10:10 NPK and 4 g L^{-1} dolomite limestone ($MgCO_3$ + $CaCO_3$). Weekly foliar fertilization was carried out using 2g/L Biofert® leaf fertilizer. Upon appearance of the first true leaf, seedlings of each genotype were transplanted to pots with a capacity of 0.7L and 3.5L for MT and M82, respectively. The new pots were filled with substrate as described above, except for the NPK supplementation, which was increased to 8 g L^{-1}. Irrigation was performed daily, twice a day, in a controlled manner, so that each vessel received the same volume of water.

Experimental setup

The two experiments were conducted in completely randomized experimental design, in 2×2 factorial, consisting of two genotypes, and two irradiance levels (sun and shade). Plants in the 'sun' treatment were exposed to greenhouse conditions, with midday irradiance of ~900 µmol photons m^{-2} s^{-1}. For the 'shade' treatment plants were maintained on a separate bench covered with neutral shade cloth, with a retention capacity of 70% of sunlight (250-300 µmol photons m^{-2} s^{-1}).

Plant morphology determinations

Morphological characterization was performed in MT plants 50 days after germination. The number of leaves to the first inflorescence was obtained by counting the number of leaves on the main stem, from the bottom up. Stem diameter was measured using a mechanical pachymeter (Mitutoyo® Vernie Caliper model, Japan) and measurements were made at the base of the plant. Total leaf area was calculated digitizing all leaves with an HP Scanjet G2410 scanner (Hewlett-Packard, Palo Alto, California, USA), and then calculating the area using ImageJ® (http://rsbweb.nih.gov/ij/). For determination of specific leaf area (SLA), the fully expanded fourth leaf was taken as the base that was collected and digitized, being obtained its area and later dried in oven at 70ºC for 72h. SLA was calculated through the relationship between leaf area (LA) and dry mass (LDW), as described by the equation:

$$SLA\ (cm^2\ g^{-1}) = LA/LDW$$

Plant growth evaluation was determined from root, stem and leaves dry mass data by destructive analysis 65 days after germination. Root, stem and leaf were collected separately and packed in paper bags and oven dried at 70°C for 72h until they reached constant weight. The samples were then weighed in a semi-analytical balance (AUY220, Shimadzu, Kyoto, Japan) with a sensitivity of 0.01 g.

Elliptical Fourier Descriptor analysis of leaflet shape

Leaflets were dissected from leaves of MT and *obv* plants grown under sun and shade conditions and scanned on a white background. From each leaf, the terminal leaflet and the two most distal leaflet pairs were isolated using binary thresholding functions in ImageJ (Abramoff et al., 2004) and converted to .bmp files for analysis in SHAPE (Iwata and Ukai, 2002), where each leaflet was converted into chaincode, oriented, and decomposed into harmonic coefficients. The harmonic coefficients were then converted into a data frame format and read into R (R Core Team, 2017). The Momocs package (Bonhomme et al., 2014) was used to visualize mean leaflet shapes from each genotype/light treatment combination. The prcomp() function was used to

perform a Principal Component Analysis (PCA) on only A and D harmonics so that only symmetric (rather than asymmetric) shape variance was considered (Iwata et al., 1998). The results were visualized using ggplot2 (Wickham, 2016).

Light microscopy analyses

All anatomical analyses were performed in plants 50 days after germination. Epidermal and leaf blade traits were determined in MT and *obv*. For vein density, epidermal pavement cell size, stomatal density, guard cells size, and stomatal index on the adaxial and abaxial faces, the fully expanded fifth leaf was used, cleared with 95% methanol for 48h followed by 100% lactic acid.) Stomatal pore area index (SPI) was calculated as (guard cell length)^2 × stomatal density for the adaxial and abaxial epidermes and then added up (Sack et al., 2003). Images obtained in a light microscope (Zeiss, Axioscope A1 model, Thornwood, NY, USA) with attached Axiovision® 105 color image capture system, were evaluated in the Image Pro-Plus® software (version 4.5, Media Cybernetics, Silver Spring, USA). Stomatal density was calculated as number of stomata per unit leaf area, stomatal index as the proportion of guard cells to total epidermal cells. Minor vein density was measured as length of minor veins (<0.05 µm diameter) per unit leaf area.

For microscopical analyses, samples were collected from the medial region of the fully expanded fifth leaf and fixed in 70% formalin-acetic acid-alcohol (FAA) solution for 48h and then stored in 70% (v/v) aqueous ethanol. The samples were embedded in historesin (Leica Microsystems, Wetzlar, Germany), cut into cross-sections (5µm) with an automated rotary microtome (RM2155, Leica Microsystems, Wetzlar, Germany) and sequentially stained with toluidine blue.

Gas exchange and chlorophyll fluorescence determinations

Gas exchange analyses were performed in MT and M82 plants at 40 and 50 days after germination, respectively. Gas exchange measurements were performed simultaneously with chlorophyll *a* fluorescence measurements in the interval from 7:00 am to 12:00 am, for three consecutive days, using an open-flow gas exchange system infrared gas analyzer (IRGA) model

LI-6400XT coupled with a fluorescence chamber (LI-Cor, Lincoln, NE, USA). All measurements were made on terminal leaflets of intact, attached leaves in the greenhouse. The analyses were performed under common conditions for photon flux density (1000 μmol m^{-2} s^{-1}, from an LED source), leaf temperature (25 ± 0.5ºC), leaf-to-air vapor pressure difference (16.0 ± 3.0 mbar), air flow rate into the chamber (500 μmol s^{-1}) and reference CO_2 concentration of 400 ppm (injected from a cartridge), using an area of 2 cm^2 in the leaf chamber. The dark respiration (R_d) determination was performed using an open-flow gas exchange system infrared gas analyzer (IRGA) model LI-6400XT coupled with a fluorescence chamber (LI-Cor, Lincoln, NE, USA), however, the plants were adapted to the dark at least 1h before the measurements, as described by Niinemets et al., 2006.

Photochemical efficiency of photosystem II (φPSII) was determined by measuring the steady-state fluorescence (Fs) and the maximum fluorescence (F_m'), using a pulse of saturating light of approximately 8000 μmol photons m^{-2} s^{-1}, as described by Genty et al. (1989). The electron transport rate (ETR) was calculated as:

$$ETR = \varphi PSII \times \beta \times \alpha \times RFA$$

Where α is the absorbance of the sheet and β reflects the partitioning of the energy packets between photosystems I and II, and αβ was determined according to Valentini et al. (1995), from the relationship between *A* and RFA x φPSII / 4 obtained by varying the light intensity under non-photorespiratory conditions. The initial fluorescence emission (F_0) was determined illuminating dark-adapted leaves (1 h) with weak modulated measuring beams (0.03 μmol m^{-2} s^{-1}). A saturating white light pulse (8000 μmol m^{-2} s^{-1}) was applied for 0.8 s to obtain the maximum fluorescence (F_m), from which the variable-to-maximum Chl fluorescence ratio, was then calculated:

$$F_v/F_m=[(F_m - F_0)/F_m)]$$

In light-adapted leaves, the steady-state fluorescence yield (F_s) was measured with the application of a saturating white light pulse (8000 μmol m^{-2} s^{-1}) to achieve the light-adapted maximum fluorescence (F_m'). Far-red illumination (2 μmol m^{-2} s^{-1}) was applied after turning off

the actinic light to measure the light-adapted initial fluorescence (F_0'). The capture efficiency of excitation energy by open photosystem II reaction centers (F_v'/F_m') was estimated following (Genty et al., 1989). We further measured the coefficients of photochemical (*qP*) and non-photochemical (*NPQ*) quenching and calculated electron transport (ETR) rates (Maxwell and Johnson, 2000)

A/C_i curves were determined initiated at an ambient [CO_2] of 400 μmol mol^{-1} under a saturating *PPFD* of 1000 μmol m^{-2} s^{-1} at 25°C under ambient O_2 supply. CO_2 concentration was decreased to 50 μmol mol^{-1} of air in step changes. Upon the completion of the measurements at low C_a, C_a was returned to 400 μmol mol^{-1} of air to restore the original *A*. Next, CO_2 was increased stepwise to 1600 μmol mol^{-1} of air. The A/C_i curves thus consist of *A* values corresponding to 12 different ambient CO_2 values. The maximum rate of carboxylation (V_{cmax}), maximum rate of carboxylation limited by electron transport (J_{max}) and triose-phosphate utilization (TPU) were estimated by fitting the mechanistic model of CO_2 assimilation proposed by (Farquhar et al., 1980). Corrections for the leakage of CO_2 into and out of the leaf chamber of the LI-6400 were applied to all gas-exchange data as described by Rodeghiero et al. (2007).

Water relations

Leaf water potential (Ψw) was measured in the central leaflet of the fifth fully expanded leaf in MT and M82 plants 40 and 50 days of age, respectively, using a Scholander-type pressure chamber (model 1000, PMS Instruments, Albany, NY, USA). The apparent hydraulic conductance (K_{leaf}) determinations were performed simultaneously as the Ψw, and their value was estimated using the transpiration rates and the water potential difference between the transpiring and non-transpiring leaflet. The non-transpiring leaflet consisted of the lateral leaflet of the same leaf, which was covered with plastic film and foil the night before the measurements. K_{leaf} was calculated according to Ohm's law:

$$K_{leaf} = E / (\Psi_L - \Psi_X)$$

Where: *E* is the transpiration rate (mmol m^{-2} s^{-1}) determined during gas exchange measurements, and (Ψ_L - Ψ_X) corresponds to the pressure gradient between the transpiring and non-transpiring leaflet (MPa). Measurements of leaf water potential (Ψw) and hydraulic conductance were performed immediately after analysis of gas exchange.

Biochemical determinations

Further biochemical analyses of the leaves were performed in MT and M82 plants 40 and 50 days after germination, respectively. The terminal leaflet of the sixth fully expanded leaf was collected around midday on a cloudless day, instantly frozen in liquid N_2 and stored at -80°C. Subsequently, the samples were lyophilized at -48°C and macerated with the aid of metal beads in a Mini-Beadbeater-96 type cell disrupter (Biospec Products, Bartlesville, OK, USA). The quantification of glucose, fructose and sucrose were performed according to Fernie et al. (2001).

Agronomic parameters (yield and Brix)

Fruit agronomic parameters were determined in MT and M82 plants 80 days after germination. The number of fruits per plant was obtained from fruit counts and the frequency of green and mature fruits was also determined separately. Fruit average weight was determined after individual weighing of each fruit, using a semi analytical balance with a sensitivity of 0.01 g (AUY220, Shimadzu, Kyoto, Japan). Yield per plant corresponds to the total weight of fruits per plant. The determination of the soluble solids content (°Brix) in the fruits was measured with a digital temperature-compensated refractometer, model RTD 45 (Instrutherm®, São Paulo, Brazil). Six ripe fruits per plant were evaluated in five replicates per genotype.

Statistical analysis

The data were subjected to analysis of variance (ANOVA) using Assistat version 7.6 (http://assistat.com) and the means were compared by the Tukey test at the 5% level of significance ($P \leq 0.05$).

Supplemental Data

Supplemental Figure 1. Leaf anatomy in tomato cv Micro-Tom (MT) and the *obscuravenosa* (*obv*) mutant.

Supplemental Figure 2. Infiltration of water + dye in MT and *obv* leaves.

Supplemental Figure 3. Heterobaric and homobaric plants in the tomato cv M82 background.

Supplemental Figure 4. Leaf hydraulic conductance in heterobaric and homobaric M82 plants.

Supplemental Figure 5. Side branching ratio in MT and *obv* plants grown in the sun and shade.

Supplemental Figure 6. Transpiration efficiency in heterobaric and homobaric plants in the tomato cv M82 background grown in the sun and shade.

Supplemental Table 1. Chlorophyll fluorescence analyses in MT and *obv* grown in two different irradiance levels (sun and shade).

Supplemental Table 2. Leaf carbohydrate and pigment content in MT and *obv* grown in sun and shade.

Supplemental Table 3. Agronomic parameters (yield and Brix) in homobaric and heterobaric plants of MT and M82 grown in the sun and shade.

Acknowledgments

This work was supported by funding from the Agency for the Support and Evaluation of Graduate Education (CAPES, Brazil), the National Council for Scientific and Technological Development (CNPq, Brazil), Foundation for Research Assistance of the São Paulo State (FAPESP, Brazil) and the Foundation for Research Assistance of the Minas Gerais State (FAPEMIG, Brazil). We thank CAPES for studentship granted to M.A.M.B. L.E.P.P. acknowledges a grant from CNPq (307040/2014-3). Research fellowships granted by CNPq to L.E.P.P. and W.L.A. are gratefully acknowledged.

Tables

Table 1. Plant material used in this study. Micro-Tom (MT) and M82 are two tomato cultivars that differ in growth habit due mostly to the presence of a mutant allele of the *DWARF* gene, which codes for a key enzyme of the brassinosteroid biosynthesis pathway. The molecular identity of *OBSCURAVENOSA* (*OBV*) is unknown. MT harbors a functional, dominant allele of *OBV*, whereas M82 is a mutant (*obv*). F1 plants are hybrids with a 50/50 MT/M82 genomic complement, differing only in the presence or absence of BSEs. The F1 plants are otherwise phenotypically indistinguishable from the M82 parent.

Parental genotype	MT	MT-*obv*	M82	F1 MT×M82	F1 MT-*obv*×M82
Plant height					
Genotype	*dwarf/dwarf*	*dwarf/dwarf*	*DWARF/DWARF*	*DWARF/dwarf*	*DWARF/dwarf*
Phenotype	Dwarf plant	Dwarf plant	Tall plant	Tall plant	Tall plant
BSEs					
Genotype	*OBV/OBV*	*obv/obv*	*obv/obv*	*OBV/obv*	*obv/obv*
Phenotype	BSEs (clear veins)	No BSEs (dark veins)	No BSEs (dark veins)	BSEs (clear veins)	No BSEs (dark veins)

Table 2. Gas exchange parameters determined in fully-expanded leaves of heterobaric (Micro-Tom, MT) and homobaric (*obscuravenosa*, *obv*) in two irradiance levels (sun/shade, 900/300 μmol photons m^{-2} s^{-1}). Values are means ± s.e.m (n=8 for A, g_s and TE_i; n=6 for other parameters). Values followed by the same letter in each row were not significantly different by Tukey test at 5% probability.

	Sun		Shade	
	MT	***obv***	**MT**	***obv***
A (μmol CO_2 m^{-2} s^{-1})	21.29 ± 1.34a	20.74 ± 1.44a	17.07 ± 0.83b	20.26 ± 0.48a
g_s (mol m^{-2} s^{-1})	0.373 ± 0.039a	0.275 ± 0.020b	0.263 ± 0.016b	0.278±0.018b
TE_i (A/g_s)	59.16 ± 3.25b	76.26 ± 2.16a	65.51 ± 2.08b	74.11 ± 3.55a
$V_{c,max}$ (μmol m^{-2} s^{-1})	82.7 ± 6.04a	80.5 ± 6.26a	66.8 ± 4.38a	72.7 ± 7.72a
J_{max} (μmol m^{-2} s^{-1})	167.5± 5.74a	155.5 ± 8.48a	133.5 ± 4.54b	133.5 ± 4.54b
TPU (μmol m^{-2} s^{-1})	12.1 ± 0.34a	11.0 ± 0.62a	9.6 ± 0.36b	10.3 ± 0.1a
R_d (μmol CO_2 m^{-2} s^{-1})	1.49 ± 0.43 a	1.80 ± 0.45 a	1.42 ± 0.38 a	1.45±0.39 a

Table 3. Plant morphological parameters evaluated 50 days after germination (dag) in heterobaric (Micro-Tom, MT) and homobaric (*obscuravenosa*, *obv*) tomatoes grown in two irradiance levels (sun/shade, 900/300 μmol photons m^{-2} s^{-1}) (n=8). Dry weight was determined through destructive analysis in plants 65 dag (n = 5). Values are means ± s.e.m (n=6). Values followed by the same letter were not significantly different by Tukey test at 5% probability.

	Sun		Shade	
	MT	***obv***	**MT**	***obv***
Plant height (cm)	9.90 ± 0.30a	10.53 ± 0.28a	10.15 ± 0.62a	10.63 ± 0.18a
Leaves to 1st inflorescence	6.75 ± 0.25a	6.50 ± 0.18a	6.62 ± 0.18a	6.75 ± 0.25a
Leaf insertion angle (°)	82.8 ± 2.32a	73.1 ± 3.50b	81.8 ± 4.30a	65.5 ± 3.72b
Stem diameter (cm)	0.40 ± 0.02a	0.38 ± 0.03a	0.28 ± 0.01b	0.28 ± 0.01b
Dry weight (g)				
Leaves	1.30 ± 0.17a	1.35 ± 0.06a	1.07 ± 0.11a	1.05 ± 0.08a
Stem	2.17 ± 0.14ab	2.49 ± 0.19ab	1.54 ± 0.18b	1.72 ± 0.07a
Roots	0.80 ± 0.06a	0.80 ± 0.04a	0.50 ± 0.03b	0.43 ± 0.04b
Total	4.28 ± 0.34ab	4.65 ± 0.28a	3.12 ± 0.32b	3.21 ± 0.14b

Figure legends

Figure 1. Irradiance level differentially alters morphology in heterobaric and homobaric leaves. A) Principal Component Analysis (PCA) on A and D harmonic coefficients from an Elliptical Fourier Descriptor (EFD) analysis shows distinct symmetric shape differences between MT and *obv* leaflets, but small differences due to light treatment. 95% confidence ellipses are provided for each genotype and light treatment combination, indicated by color. B) Mean leaflet shapes for MT and *obv* in each light treatment. Mean leaflet shapes are superimposed for comparison. Note the wider *obv* leaflet compared to MT. MT shade, red; MT sun, green; *obv* shade, blue; *obv* sun, purple. C) Specific leaf area (SLA); D-E) relationship between perimeter/area and perimeter^2/area. Bars are mean values ± s.e.m. (n=5). Different letters indicate significant differences by Tukey's test at 5% probability.

Figure 2. Tomato homobaric leaves show reduced hydraulic conductance (K_{leaf}) compared to heterobaric leaves when grown in the sun, but not in the shade. A) Leaf hydraulic conductance in cv Micro-Tom (MT, heterobaric) and the *obscuravenosa* mutant (*obv*, homobaric) leaves from plants grown in either sun or shade conditions. B) The same measurement but in tomato cv M82 compared to its isogenic line *obv*. Bars are mean values ± s.e.m. (n=3 for A and n=5 for B). Different letters indicate significant differences by Tukey's test at 5% probability.

Figure 3. Homobaric leaves maintain lower stomatal conductance in both sun and shade conditons. Relationship between photosynthetic CO_2 assimilation rate (A) and stomatal conductance (g_s) for Micro-Tom (MT) and the *obscuravenosa* (*obv*) mutant plants grown in the sun (A) or shade (B). A rectangular hyperbolic function was fitted in each panel. Each point corresponds to an individual measurement carried out at common conditions in the leaf chamber: photon flux density (1000 μmol m^{-2} s^{-1}, from an LED source), leaf temperature (25 ± 0.5ºC), leaf-to-air vapor pressure difference (16.0 ± 3.0 mbar), air flow rate into the chamber (500 μmol s^{-1}) and reference CO_2 concentration of 400 ppm (injected from a cartridge), using an area of 2 cm^2 in the leaf chamber.

Figure 4. Stomatal traits are differentially affected by irradiance in heterobaric and homobaric tomato leaves. A) SPI: stomatal pore area index, calculated as (guard cell length)^2 × stomatal density for the adaxial and abaxial epidermes and then added up; B) Guard cell length; C-D) Stomatal density, number of stomata per unit leaf area; All histograms show mean values ± s.e.m. (n=6). Different letters indicate significant differences by Tukey's test at 5% probability.

Figure 5. Irradiance level differentially alters leaf anatomical parameters in heterobaric and homobaric leaves. A) Representative cross-sections of tomato cv Micro-Tom (MT, heterobaric) and the *obscuravenosa* mutant (*obv*, homobaric) leaves from plants grown in either sun or shade. The background was removed for clarity. PP: palisade parenchyma; SP: spongy parenchyma; IAS: intercellular air spaces; AE: abaxial epidermis. B) Representative plates showing the pattern and density of minor veins in 7.8 mm^2 sections in mature, cleared leaves. Scale bar=200 μm. C-G) Histograms with mean values ± s.e.m. (n=6) for the ratio between palisade and spongy parenchyma thickness; thickness of the abaxial epidermis; the proportion of intercellular air spaces and the density of minor (quaternary and higher order) veins measured in cleared sections of the leaves and lamina thickness. Different letters indicate significant differences by Tukey's test at 5% probability.

Figure 6. Reaction norms of structural and physiological traits in relation to leaf thickness in two irradiance levels in homobaric and heterobaric leaves. A) light-saturated photosynthetic assimilation rate (A); B) proportion of intercellular air spaces in the lamina, C) minor vein per unit leaf area (VLA) and D) stomatal pore area index (adimensional). The values of the slopes are shown next to each line.

Figure 7. **Hypothetical model showing the influence of bundle sheath extensions (BSEs) on leaf anatomical and physiological traits in response to irradiance**. BSEs were the independent variable in this work (green). Traits affected by the presence or absence of BSEs in response to changes in growth irradiance are shown in blue. Traits measured and not affected are shown in open boxes and traits not measured in this study are in grey. Vein density in our study refers to minor vein length per unit leaf area. K_x, K_{ox} hydraulic conductance in the xylem and outside the xylem, respectively. K_{leaf}, K_{plant}, leaf and plant hydraulic conductance. Ψ, water potential; Ψ_{leaf}, leaf water potential; g_{max}, maximum stomatal conductance; gs, stomatal conductance; g_m, mesophyll conductance; C_c, chloroplastic CO_2 concentration; Vcmax, maximum CO2 carboxylation rate; Jmax, electron transport rate; SLA, specific leaf area; LT, LD, LL, leaf thickness, density and lifespan; SPI, stomatal pore area index. See text for detailed definitions of each parameter.

LITERATURE CITED

Abramoff MD, Magalhães PJ, Ram SJ (2004) Biophotonics international. Biophotonics Int **11**: 36–42

Bonhomme V, Picq S, Gaucherel C, Claude J, Bonhomme V, Picq S, Gaucherel C, Claude J (2014) Momocs: Outline Analysis Using R. J Stat Softw **56**: 1–24

Brodribb TJ (2009) Xylem hydraulic physiology: The functional backbone of terrestrial plant productivity. Plant Sci **177**: 245–251

Brodribb TJ, Feild TS, Jordan GJ (2007) Leaf maximum photosynthetic rate and venation are linked by hydraulics. Plant Physiol **144**: 1890–1898

Brodribb TJ, Jordan GJ (2011) Water supply and demand remain balanced during leaf acclimation of Nothofagus cunninghamii trees. New Phytol **192**: 437–448

Buckley TN, John GP, Scoffoni C, Sack L (2015) How does leaf anatomy influence water transport outside the xylem? Plant Physiol **168**: 1616–1635

Buckley TN, Sack L, Farquhar GD (2016) Optimal plant water economy. Plant Cell Environ **40**: 881–896

Buckley TN, Sack L, Gilbert ME (2011) The role of bundle sheath extensions and life form in stomatal responses to leaf water status. Plant Physiol **156**: 962–973

Campos ML, Carvalho RF, Benedito VA, Peres LEP (2010) Small and remarkable. The Micro-Tom model system as a tool to discover novel hormonal functions and interactions.

Plant Signal Behav **5**: 1–4

Carins Murphy M, Dow G, Jordan G, Brodribb T (2017) Vein density is independent of epidermal cell size in Arabidopsis mutants. Funct Plant Biol **44**: 410–418

Carvalho RF, Campos ML, Pino LE, Crestana SL, Zsögön A, Lima JE, Benedito VA, Peres LE (2011) Convergence of developmental mutants into a single tomato model system: "Micro-Tom" as an effective toolkit for plant development research. Plant Methods **7**: 18

Chitwood DH, Headland LR, Ranjan A, Martinez CC, Braybrook SA, Koenig DP, Kuhlemeier C, Smith RS, Sinha NR (2012) Leaf asymmetry as a developmental constraint imposed by auxin-dependent phyllotactic patterning. Plant Cell **24**: 2318–2327

Chitwood DH, Kumar R, Ranjan A, Pelletier JM, Townsley BT, Ichihashi Y, Martinez CC, Zumstein K, Harada JJ, Maloof JN, et al (2015) Light-induced indeterminacy alters shade-avoiding tomato leaf morphology. Plant Physiol **169**: 2030–2047

Cochard H, Venisse J-S, Barigah TS, Brunel N, Herbette S, Guilliot A, Tyree MT, Sakr S (2007) Putative role of aquaporins in variable hydraulic conductance of leaves in response to light. Plant Physiol **143**: 122–133

Esau K (1977) Anatomy of Seed Plants, 2nd ed. John Wiley & Sons, Inc., New York

Evans JR, vonCaemmerer S (1996) Carbon dioxide diffusion inside leaves. Plant Physiol **110**: 339–346

Farquhar GD, von Caemmerer S, Berry JA (1980) A biochemical model of photosynthetic CO2 assimilation in leaves of C3 species. Planta **149**: 78–90

Fernie AR, Roscher A, Ratcliffe RG, Kruger NJ (2001) Fructose 2,6-bisphosphate activates pyrophosphate: Fructose-6-phosphate 1-phosphotransferase and increases triose phosphate to hexose phosphate cycling heterotrophic cells. Planta **212**: 250–263

Flexas J, Niinemets Ü, Gallé A, Barbour MM, Centritto M, Diaz-Espejo A, Douthe C, Galmés J, Ribas-Carbo M, Rodriguez PL, et al (2013) Diffusional conductances to CO2 as a target for increasing photosynthesis and photosynthetic water-use efficiency. Photosynth Res **117**: 45–59

Genty B, Briantais J-M, Baker NR (1989) The relationship between the quantum yield of photosynthetic electron transport and quenching of chlorophyll fluorescence. Biochim Biophys Acta - Gen Subj **990**: 87–92

Guyot G, Scoffoni C, Sack L (2012) Combined impacts of irradiance and dehydration on leaf hydraulic conductance: insights into vulnerability and stomatal control. Plant Cell Environ **35**: 857–871

Hacker J, Neuner G (2007) Ice propagation in plants visualized at the tissue level by infrared differential thermal analysis (IDTA). Tree Physiol **27**: 1661–1670

Inoue Y, Kenzo T, Tanaka-Oda A, Yoneyama A, Ichie T (2015) Leaf water use in heterobaric and homobaric leafed canopy tree species in a Malaysian tropical rain forest. Photosynthetica **53**: 177–186

Iwata H, Niikura S, Matsuura S, Takano Y, Ukai Y (1998) Evaluation of variation of root shape of Japanese radish (*Raphanus sativus* L.) based on image analysis using elliptic Fourier descriptors. Euphytica **102**: 143–149

Iwata H, Ukai Y (2002) SHAPE: A computer program package for quantitative evaluation of biological shapes based on elliptic Fourier descriptors. J Hered **93**: 384–385

Jones CM, Rick CM, Adams D, Jernstedt J, Chetelat RT (2007) Genealogy and fine mapping of Obscuravenosa, a gene affecting the distribution of chloroplasts in leaf veins and evidence of selection during breeding of tomatoes (*Lycopersicon esculentum*; Solanaceae). Am J Bot **94**: 935–947

Karabourniotis G, Bornman JF, Nikolopoulos D (2000) A possible optical role of the bundle sheath extensions of the heterobaric leaves of *Vitis vinifera* and *Quercus coccifera*. Plant, Cell Environ **23**: 423–430

Kenzo T, Ichie T, Watanabe Y, Hiromi T (2007) Ecological distribution of homobaric and heterobaric leaves in tree species of Malaysian lowland tropical rainforest. Am J Bot **94**: 764–775

Lambers H, Chapin FSIII, Pons TL (2008) Plant Physiological Ecology. Springer Verlag, New York City

Laur J, Hacke UG (2013) Transpirational demand affects aquaporin expression in poplar roots. J Exp Bot **64**: 2283–2293

Lawson T, Morison J (2006) Visualising patterns of CO2 diffusion in leaves. New Phytol **169**: 641–643

Leegood RC (2008) Roles of the bundle sheath cells in leaves of C3 plants. J Exp Bot **59**: 1663–1673

Liakoura V, Fotelli MN, Rennenberg H, Karabourniotis G (2009) Should structure-function relations be considered separately for homobaric vs. heterobaric leaves? Am J Bot **96**: 612–619

Lloyd J, Bloomfield K, Domingues TF, Farquhar GD (2013) Photosynthetically relevant foliar traits correlating better on a mass vs an area basis: of ecophysiological relevance or just a case of mathematical imperatives and statistical quicksand? New Phytol **199**: 311–321

Martins SC V., Galmés J, Cavatte PC, Pereira LF, Ventrella MC, DaMatta FM (2014) Understanding the low photosynthetic rates of sun and shade coffee leaves: bridging the gap on the relative roles of hydraulic, diffusive and biochemical constraints to photosynthesis. PLoS One **9**: e95571

Maxwell K, Johnson GN (2000) Chlorophyll fluorescence - a practical guide. J Exp Bot **51**: 659–668

Nicotra AB, Cosgrove MJ, Cowling A, Schlichting CD, Jones CS (2008) Leaf shape linked to photosynthetic rates and temperature optima in South African Pelargonium species. Oecologia **154**: 625–635

Nicotra AB, Leigh A, Boyce CK, Jones CS, Niklas KJ, Royer DL, Tsukaya H (2011) The evolution and functional significance of leaf shape in the angiosperms. Funct Plant Biol **38**: 535–552

Niinemets Ü, Cescatti A, Rodeghiero M, Tosens T (2006) Complex adjustments of photosynthetic potentials and internal diffusion conductance to current and previous light availabilities and leaf age in Mediterranean evergreen species *Quercus ilex*. Plant Cell Environ **29**: 1159–1178

Niklas KJ (1992) Plant Biomechanics: An Engineering Approach to Plant Form and Function. University of Chicago Press

Nikolopoulos D, Liakopoulos G, Drossopoulos I, Karabourniotis G (2002) The relationship between anatomy and photosynthetic performance of heterobaric leaves. Plant Physiol **129**: 235–243

Oguchi R, Hikosaka K, Hirose T (2003) Does the photosynthetic light-acclimation need change in leaf anatomy? Plant Cell Environ **26**: 505–512

Oguchi R, Hikosaka K, Hirose T (2005) Leaf anatomy as a constraint for photosynthetic acclimation: differential responses in leaf anatomy to increasing growth irradiance among three deciduous trees. Plant Cell Environ **28**: 916–927

Oguchi R, Hikosaka K, Hiura T, Hirose T (2006) Leaf anatomy and light acclimation in woody seedlings after gap formation in a cool-temperate deciduous forest. Oecologia **149**: 571–582

Ohtsuka A, Sack L, Taneda H (2017) Bundle sheath lignification mediates the linkage of leaf hydraulics and venation. Plant Cell Environ 10.1111/pce.13087

Pieruschka R, Schurr U, Jensen M, Wolff WF, Jahnke S (2006) Lateral diffusion of CO2 from shaded to illuminated leaf parts affects photosynthesis inside homobaric leaves. New Phytol **169**: 779–787

Prado K, Maurel C (2013) Regulation of leaf hydraulics: from molecular to whole plant levels. Front Plant Sci **4**: 255

Read J, Stokes A (2006) Plant biomechanics in an ecological context. Am J Bot **93**: 1546–1565

Rodeghiero M, Niinemets Ü, Cescatti A (2007) Major diffusion leaks of clamp-on leaf cuvettes still unaccounted: How erroneous are the estimates of Farquhar et al. model parameters? Plant Cell Environ **30**: 1006–1022

Sack L, Cowan PD, Jaikumar N, Holbrook NM (2003) The 'hydrology' of leaves: co-ordination of structure and function in temperate woody species. Plant Cell Environ **26**, 1343– 1356.

Sack L, Frole K (2006) Leaf structural diversity is related to hydraulic capacity in tropical rain forest trees. Ecology **87**: 483–491

Sack L, Holbrook NM (2006) Leaf hydraulics. Annu Rev Plant Biol **57**: 361–381

Sack L, Scoffoni C (2013) Leaf venation: structure, function, development, evolution, ecology and applications in the past, present and future. New Phytol **198**: 983–1000

Sack L, Scoffoni C, McKown AD, Frole K, Rawls M, Havran JC, Tran H, Tran T (2012) Developmentally based scaling of leaf venation architecture explains global ecological patterns. Nat Commun **3**: 837

Scoffoni C (2015) Modelling the outside-xylem hydraulic conductance: towards a new understanding of leaf water relations. Plant Cell Environ **38**: 4–6

Scoffoni C, Kunkle J, Pasquet-Kok J, Vuong C, Patel AJ, Montgomery RA, Givnish TJ, Sack L (2015) Light-induced plasticity in leaf hydraulics, venation, anatomy, and gas exchange in ecologically diverse Hawaiian lobeliads. New Phytol **207**: 43–58

Scoffoni C, Pou AL, Cia, Aasamaa KR, Sack L (2008) The rapid light response of leaf hydraulic conductance: new evidence from two experimental methods. Plant Cell Environ **31**: 1803–1812

Terashima I (1992) Anatomy of nonuniform leaf photosynthesis. Photosynth Res **31**: 195–212

Valentini R, Epron D, Angelis PDE, Matteucci G, Dreyer E (1995) In situ estimation of net CO_2 assimilation, photosynthetic electron flow and photorespiration in Turkey oak (*Q. cerris* L.) leaves: diurnal cycles under different levels of water supply. Plant Cell Environ **18**: 631–640

Wellburn AR (1994) The spectral determination of chlorophylls a and b, as well as total carotenoids, using various solvents with spectrophotometers of different resolution. J Plant Physiol **144**: 307–313

Wickham H (2016) ggplot2: elegant graphics for data analysis, 2nd ed. Springer

Wylie RB (1952) The bundle sheath extension in leaves of dicotyledons. Am J Bot **39**: 645–651

Zsögön A, Alves Negrini AC, Peres LEP, Nguyen HT, Ball MC (2015) A mutation that

eliminates bundle sheath extensions reduces leaf hydraulic conductance, stomatal conductance and assimilation rates in tomato (*Solanum lycopersicum*). New Phytol **205**: 618–626

Zwieniecki MA, Brodribb TJ, Holbrook NM (2007) Hydraulic design of leaves: insights from rehydration kinetics. Plant Cell Environ **30**: 910–921

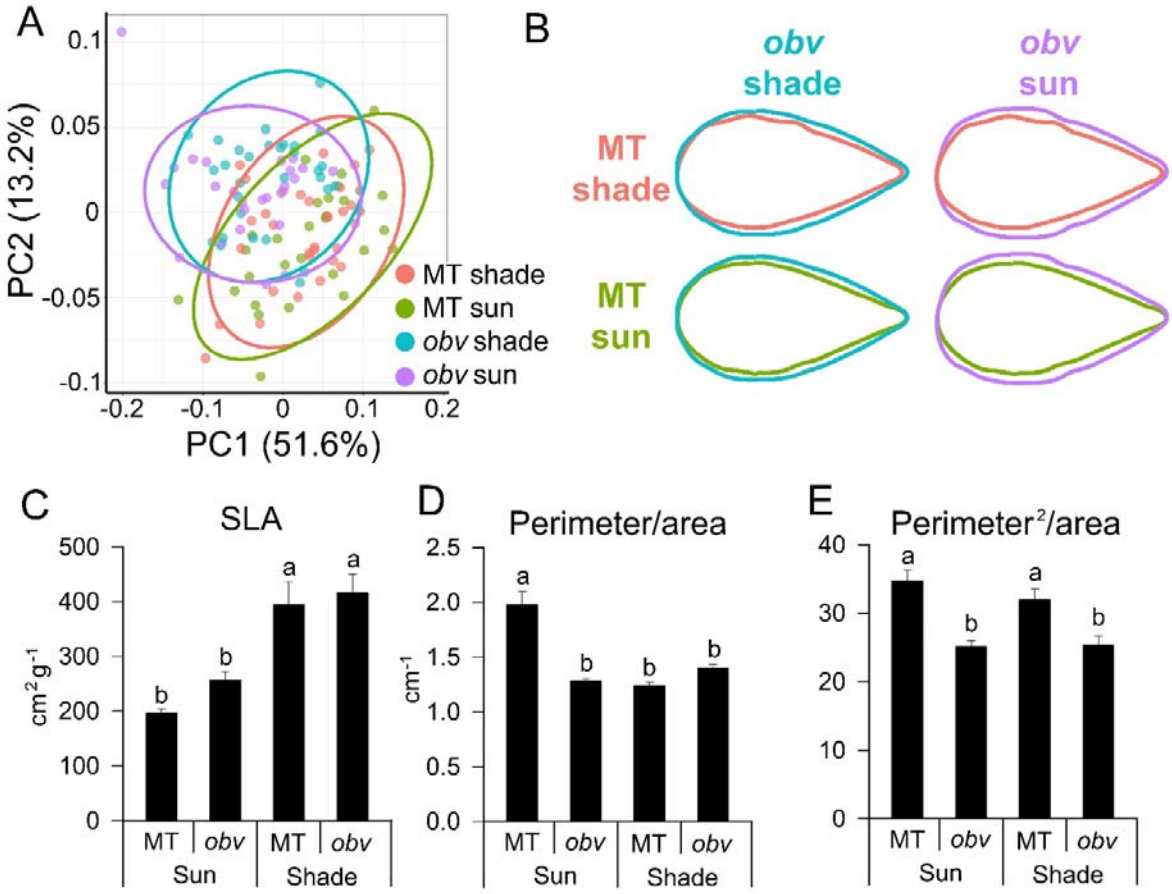

Figure 1. Irradiance level differentially alters morphology in heterobaric and homobaric leaves. (A) Principal Component Analysis (PCA) on A and D harmonic coefficients from an Elliptical Fourier Descriptor (EFD) analysis shows distinct symmetric shape differences between MT and *obv* leaflets, but small differences due to light treatment. 95% confidence ellipses are provided for each genotype and light treatment combination, indicated by color. (B) Mean leaflet shapes for MT and *obv* in each light treatment. Mean leaflet shapes are superimposed for comparison. Note the wider *obv* leaflet compared to MT. MT shade, red; MT sun, green; *obv* shade, blue; *obv* sun, purple. (C) Specific leaf area (SLA); (D-E) relationship between perimeter/area and perimeter^2/area. Bars are mean values ± s.e.m. (n=5). Different letters indicate significant differences by Tukey's test at 5% probability.

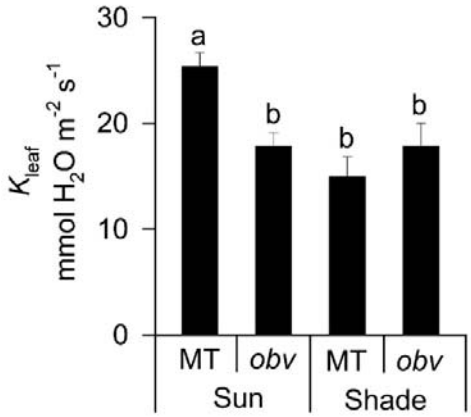

Figure 2. Tomato homobaric leaves show reduced hydraulic conductance (K_{leaf}) compared to heterobaric leaves when grown in the sun, but not in the shade. Leaf hydraulic conductance in cv Micro-Tom (MT, heterobaric) and the *obscuravenosa* mutant (*obv*, homobaric) leaves from plants grown in either sun or shade conditions. Bars are mean values ± s.e.m. (n=3). Different letters indicate significant differences by Tukey's test at 5% probability.

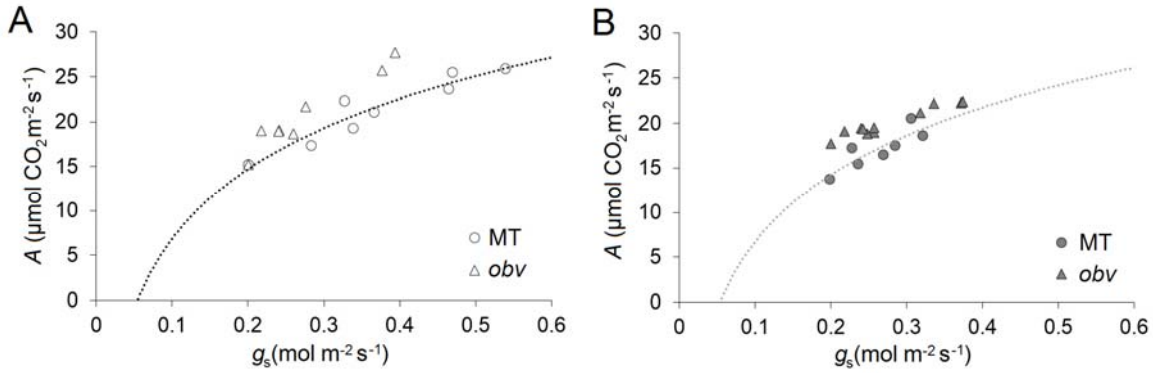

Figure 3. Homobaric leaves maintain lower stomatal conductance in both sun and shade conditions. Relationship between photosynthetic CO_2 assimilation rate (*A*) and stomatal conductance (g_s) for Micro-Tom (MT) and the *obscuravenosa* (*obv*) mutant plants grown in the sun (A) or shade (B). A rectangular hyperbolic function was fitted in each panel. Each point corresponds to an individual measurement carried out at common conditions in the leaf chamber: photon flux density (1000 µmol m^{-2} s^{-1}, from an LED source), leaf temperature (25 ± 0.5ºC), leaf-to-air vapor pressure difference (16.0 ± 3.0 mbar), air flow rate into the chamber (500 µmol s^{-1}) and reference CO_2 concentration of 400 ppm (injected from a cartridge), using an area of 2 cm^2 in the leaf chamber.

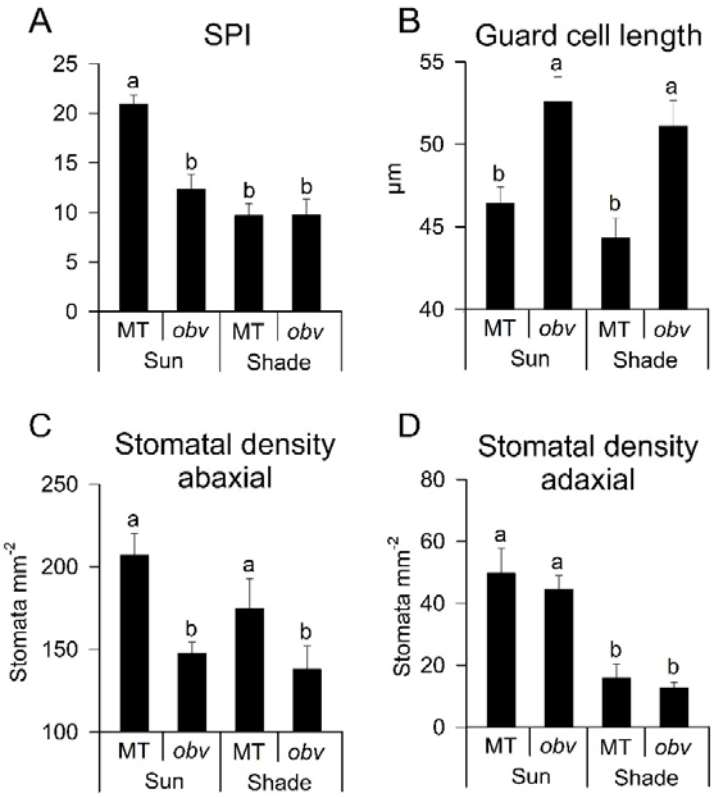

Figure 4. Stomatal traits are differentially affected by irradiance in heterobaric and homobaric tomato leaves. (A) SPI: stomatal pore area index, calculated as (guard cell length)^2 × stomatal density for the adaxial and abaxial epidermes and then added up; (B) Guard cell length; (C-D) Stomatal density, number of stomata per unit leaf area; All histograms show mean values ± s.e.m. (n=6). Different letters indicate significant differences by Tukey's test at 5% probability.

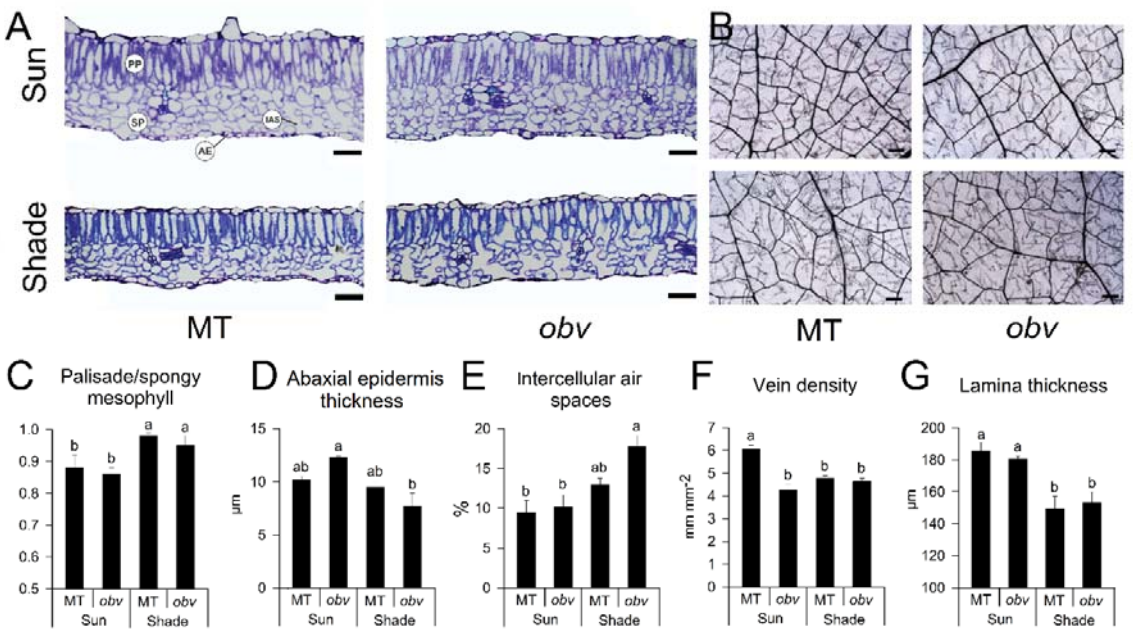

Figure 5. Irradiance level differentially alters leaf anatomical parameters in heterobaric and homobaric leaves. (A) Representative cross-sections of tomato cv Micro-Tom (MT, heterobaric) and the *obscuravenosa* mutant (*obv*, homobaric) leaves from plants grown in either sun or shade. The background was removed for clarity. PP: palisade parenchyma; SP: spongy parenchyma; IAS: intercellular air spaces; AE: abaxial epidermis. (B) Representative plates showing the pattern and density of minor veins in 7.8 mm^2 sections in mature, cleared leaves. Scale bar=200 µm. (C-G) Histograms with mean values ± s.e.m. (n=6) for the ratio between palisade and spongy parenchyma thickness; thickness of the abaxial epidermis; the proportion of intercellular air spaces and the density of minor (quaternary and higher order) veins measured in cleared sections of the leaves and lamina thickness. Different letters indicate significant differences by Tukey's test at 5% probability.

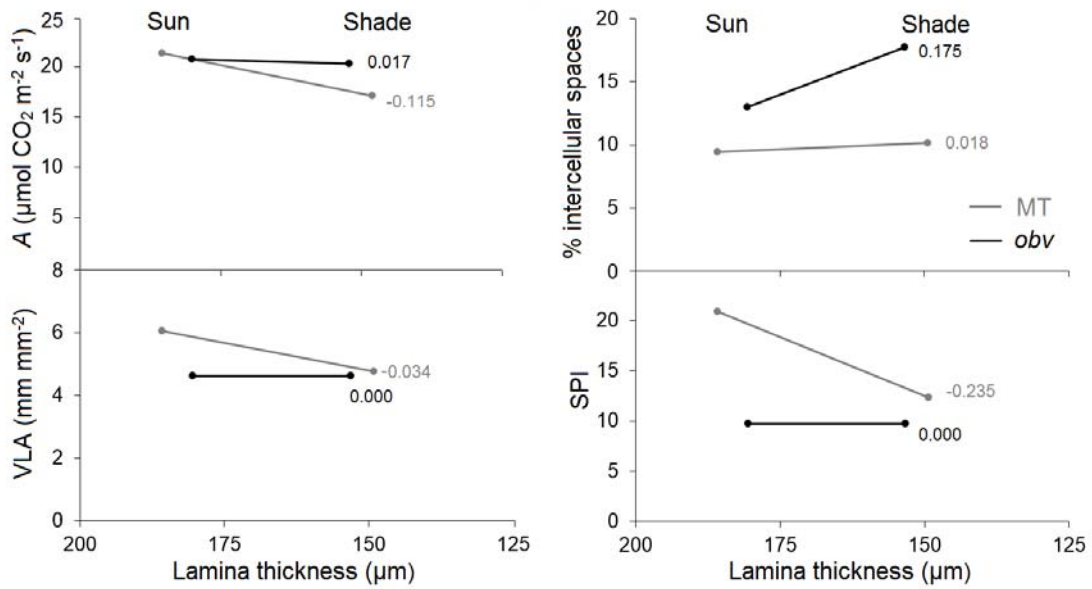

Figure 6. Reaction norms of structural and physiological traits in relation to leaf thickness in two irradiance levels in homobaric and heterobaric leaves. (A) light-saturated photosynthetic assimilation rate (*A*); (B) proportion of intercellular air spaces in the lamina, (C) minor vein per unit leaf area (VLA) and (D) stomatal pore area index (adimensional). The values of the slopes are shown next to each line.

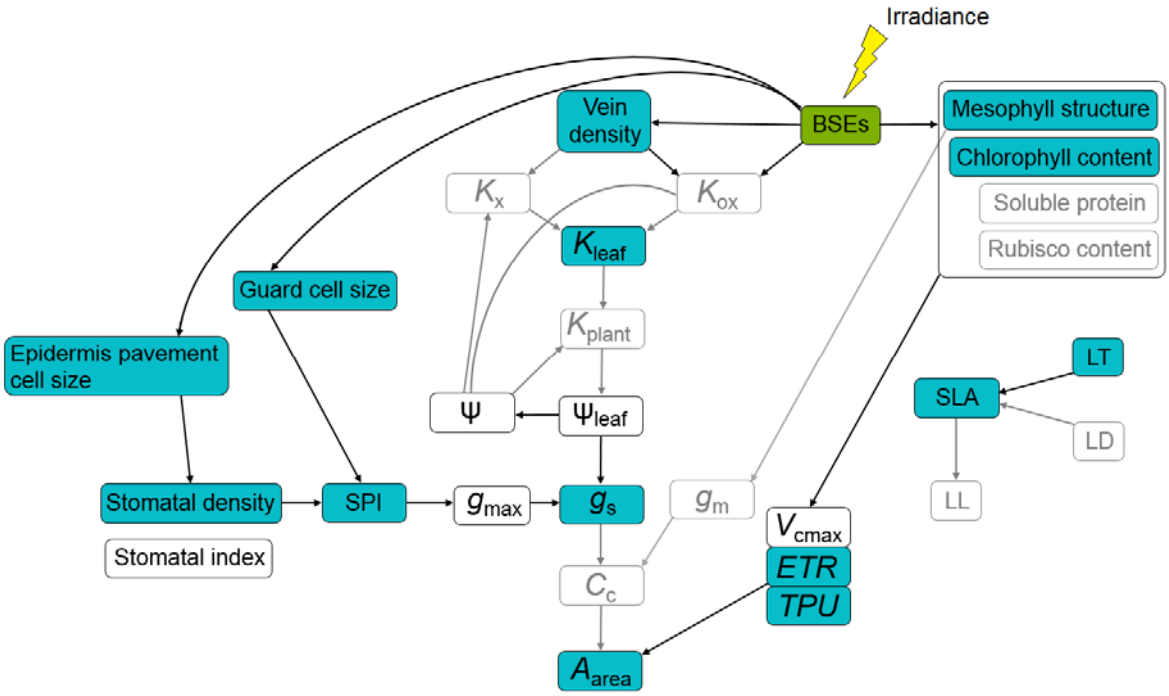

Figure 7. **Hypothetical model showing the influence of bundle sheath extensions (BSEs) on leaf anatomical and physiological traits in response to irradiance**. BSEs were the independent variable in this work (green). Traits affected by the presence or absence of BSEs in response to changes in growth irradiance are shown in blue. Traits measured and not affected are shown in open boxes and traits not measured in this study are in grey. Vein density in our study refers to minor vein length per unit leaf area. K_x, K_{ox} hydraulic conductance in the xylem and outside the xylem, respectively. K_{leaf}, K_{plant}, leaf and plant hydraulic conductance. Ψ, water potential; Ψ_{leaf}, leaf water potential; g_{max}, maximum stomatal conductance; gs, stomatal conductance; g_m, mesophyll conductance; C_c, chloroplastic CO_2 concentration; Vcmax, maximum CO2 carboxylation rate; Jmax, electron transport rate; SLA, specific leaf area; LT, LD, LL, leaf thickness, density and lifespan; SPI, stomatal pore area index. See text for detailed definitions of each parameter.